Orthogonal neural representations support perceptual judgements of natural stimuli

Authors: Ramanujan Srinath[1,2], Amy M. Ni[1,2,3], Claire Marucci[3], Marlene R. Cohen[2,4], David H. Brainard[3,4]

[1] = equal contribution

[2] = Department of Neurobiology and Neuroscience Institute, The University of Chicago, Chicago, IL 60637, USA

[3] = Department of Psychology, University of Pennsylvania, Philadelphia, PA 19104, USA

[4] = equal contribution

Corresponding Author: David H. Brainard (brainard@psych.upenn.edu)

Summary

In natural behavior, observers must separate relevant information from a barrage of irrelevant information. Many studies have investigated the neural underpinnings of this ability using artificial stimuli presented on simple backgrounds. Natural viewing, however, carries a set of challenges that are inaccessible using artificial stimuli, including neural responses to background objects that are task-irrelevant. An emerging body of evidence suggests that the visual abilities of humans and animals can be modeled through the linear decoding of task-relevant information from visual cortex. This idea suggests the hypothesis that irrelevant features of a natural scene should impair performance on a visual task only if their neural representations intrude on the linear readout of the task relevant feature, as would occur if the representations of task-relevant and irrelevant features are not orthogonal in the underlying neural population. We tested this hypothesis using human psychophysics and monkey neurophysiology, in response to parametrically variable naturalistic stimuli. We demonstrate that 1) the neural representation of one feature (the position of a central object) in visual area V4 is orthogonal to those of several background features, 2) the ability of human observers to precisely judge object position was largely unaffected by task-irrelevant variation in those background features, and 3) many features of the object and the background are orthogonally represented by V4 neural responses. Our observations are consistent with the hypothesis that orthogonal neural representations support stable perception of objects and features despite the tremendous richness of natural visual scenes.

Keywords

neural representations, decoding, vision, psychophysics, population recordings, V4, natural vision

Introduction

A major function of the visual system as it supports thought and action is to infer properties of currently relevant stimuli, while at the same time ignoring the tremendous amount of task-irrelevant information that bombards our retinas. For example, choosing a banana to pick from a tree involves judging its location and ripeness and largely ignoring the surrounding leaves, trunk, clouds in the sky, animals, plants, other objects, and a host of ever-changing visual stimulation that could distract from the task at hand.

Most laboratory studies of the neural basis of visual perception and the ability to focus on task-relevant information use, for good reasons, artificial stimuli on simplified backgrounds[1–9]. Our own studies have measured the ability to ignore distractors by training monkeys to alternate attention between two simple Gabor stimuli on a gray background[10–16]. The advantage of these reduced experimental designs is rigor and experimental control: one can parametrically vary stimuli and precisely quantify the input to the visual system.

The downside of using reduced artificial stimuli, besides a lack of naturalism, is that their very simplicity prevents them from fully illuminating the neural algorithms by which the brain sorts through the large quantity of ever-changing visual information that is characteristic of natural visual experience (see simulations in Ruff et al, 2018[12]). For example, decoding the location of a Gabor stimulus on a gray background can be accomplished using any number of neural algorithms. Essentially all neurons in any visual cortical area will fire more spikes when a Gabor stimulus is in their receptive field than to a uniform gray background. One could infer the location of the Gabor, therefore, using many different linear or nonlinear functions of the responses of neurons selected

from many combinations of brain areas[17–22]. Not all these functions, however, would be expected generalize well to a more naturalistic position-decoding task.

Decoding the position of a banana embedded in a naturalistic scene poses a richer perceptual problem. Some neurons will modulate more to changes in background branches, leaves, or other stimuli than to changes in the position the banana. And visual neurons are tuned for multiple features, meaning that a moderate response from one neuron might indicate the presence of the neuron's preferred color (e.g. the yellow of a ripe banana) at a non-preferred location (barely overlapping its receptive field) or a non-preferred color (e.g. the green of a leaf) at its preferred location. Single neurons therefore provide ambiguous information about where a ripe banana might be. This ambiguity can be overcome using combinations of neurons with particular tuning properties, but the set of appropriate neural weighting functions is more constrained than for the case of simpler stimuli[12].

This intuition can be formalized by considering a high-dimensional neural-response space in which each dimension represents the firing rate of one neuron[23,24] The response of the entire population at any given moment (e.g. in response to one visual scene) is a point in this space. Systematically varying one scene feature, such as the position of a banana, would trace out a continuous trajectory in the response space, which can typically be approximated by a line[25,26]. If just one scene feature varies, then the current state of that feature can be read out by projecting the neural population response onto this line. If two features can vary, however, whether they can be disambiguated depends on the degree to which their variation traces out similar lines in the neural-response space. For example, variation of location and color can be disambiguated if they trace out orthogonal lines.

The number of neurons in each cortical visual area exceeds the plausible number of natural scene features, suggesting that each feature could be represented in a manner orthogonal to every other feature[27]. There is redundancy in neural tuning properties, however, so the effective dimensionality of cortical population responses tends to be much lower than the number of neurons[28–41]. In addition, any group of neurons may be sensitive to variation in a non-trivial number of visual features. For example, neurons in mid-level area V4 are known to be sensitive to multiple image features, including object location, color, luminance, contrast, curvature, texture, orientation, spatial frequency, and depth as well as to properties of the background[42–55]. The low effective dimensionality of population neural responses and the number of features they must encode make it possible that representations of different features are not orthogonal in early visual areas.

We reasoned that variation in task-irrelevant features of a natural scene should impair performance on a visual task if two conditions are met: visual information is read out of a neural population in a way that approximates a linear decoder, and the representations of relevant and irrelevant features are not orthogonal in the relevant neural populations. An emerging body of work supports the idea that the visual abilities of humans and animals can be approximated by linearly decoding the neural representation of task-relevant information[53,56–62], but the relationship between these abilities and the orthogonality of the representations of relevant and irrelevant stimulus feature values in natural scenes is largely unexplored.

Here, we leverage the power of computer graphics to take parametric control of stimulus features in naturalistic stimuli, enabling us to vary many naturalistic stimulus dimensions and test the hypothesis that the observers' perceptual abilities will not be perturbed by task-irrelevant

variations in stimuli and backgrounds if the neural representations of task-relevant and irrelevant features are orthogonal. Using a combination of human psychophysics and monkey neurophysiology, we demonstrate that 1) the population representation of object position in V4 is orthogonal to those of several background features, 2) the ability of human subjects to make precise perceptual judgments about object position was largely unaffected by task-irrelevant variation in those background features, and 3) many features of the object and the background (position, color, luminance, rotation, and depth) are independently decodable from V4 population responses. Together, these observations support the idea that orthogonal representations enable stable perception of objects and features despite the tremendous irrelevant variation inherent in natural scenes.

Results

Central hypothesis: orthogonal representations enable observers to ignore irrelevant visual information

We tested the hypothesis that task-irrelevant information will not affect a perceptual judgment if the representations of the task-relevant and irrelevant features are orthogonal. Figure 1A, B depict how we used computer graphics to parametrically vary different scene features, such as the position of a central banana, the rotational position of objects in the background, and the depth position of objects in the background. Using this set of stimulus variations, consider the effect of varying the position of the banana on the neural population response as illustrated in the left panel of Fig. 1C. Each point in the plot represents the noisy population response to one presentation of an image, illustrating how varying banana position against a fixed background can trace out a line in the high-dimensional neural population space. For this background, the position of the background could be read out by projecting the population response onto the line shown (labeled 'position axis for one background' in the figure). The middle panel of 1C shows a way that varying the background objects could affect this line in an orthogonal manner. Here the line tracing out the neural population response to the banana at various positions is shifted in a direction orthogonal to the position axis shown in the left panel. Although a different line is swept out by varying banana position against this second background, projecting onto the line for the first background continues to accurately decode the banana position. If, on the other hand, changing the background causes a change in the position axis that is not orthogonal (right panel of 1C), projecting onto the line for the first background will not provide an accurate linear position readout. Thus we test the hypothesis that changing an irrelevant feature of the background (e.g. the position of background objects) will not impact perception of the task-relevant feature if the irrelevant background changes are orthogonal to the relevant ones (Fig. 1C middle).

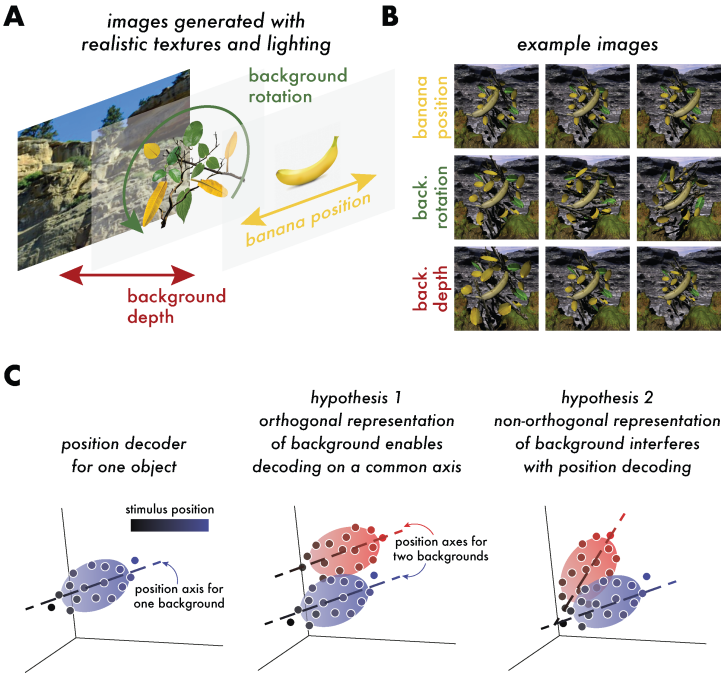

Figure 1: Stimulus design and hypotheses about how neural representations enable generalizable decoding.
A: We generated photorealistic images with permuted central object (the banana) and background properties using a Blender-based image generation pipeline that gave us control over central- and background-object properties (their position, size, pose, color, depth, luminance, etc.)
B: Example images showing variations in three parameters – central-object position in the horizontal direction, a rotation of the background objects (leaves and branches), and the depth of the background objects. Five values of each of the three parameters were chosen for each monkey based on receptive field properties (see below), yielding an image set of 5x5x5=125 images.
C: Hypothesized implications of the neural formatting of visual information on the ability to decode a visual feature. Consider the responses of a population of neurons in a high-dimensional space in which the response of each neuron is one dimension. The population responses to a series of stimuli that differ only in one parameter (e.g. the position of the central object) changes smoothly in this space (left). Responses to a set of stimuli that differ in the same parameter but also have, for example, a difference in the background will trace out a different path in this space (e.g. the red points in the center and right panels). Relative to the first (blue) path, changing the same parameter on a different background could change the population response in a parallel way; more specifically, changing the background could move the population along a dimension that is orthogonal to the dimension encoding the parameter of interest (center). This scenario would enable linear decoding of the parameter of interest that is invariant to changes in the background. Alternatively, the direction that encodes of the parameter of interest could depend on the background, suggesting that varying the background would impair the ability of a population of neurons or a psychophysical subject to estimate the parameter of interest (right).

Naturalistic stimuli with parameterizable properties

To test these predictions, we created naturalistic stimuli that had many parameterizable features (Fig. 1A, B). We parametrically varied the position of a central object (banana), and the rotation and depth of background objects (leaves and branches) set against a larger fixed contextual scene (rocks, moss-covered stumps, mountains, and skyline). We presented these stimuli within the joint receptive fields of the recorded V4 neurons (Supplementary Figure 1) while each of two monkeys fixated on a central point. In sum, we recorded V4 responses in 26 experimental sessions across two animals (85-94 visually responsive multiunits per session).

V4 neurons robustly encode stimulus position for each stimulus background

We first measured the extent to which V4 neurons encode banana position by linearly decoding that position for each unique background stimulus. Figure 2 shows that for each unique background configuration (rotation and depth), V4 neurons from a single session support linear decoding of the position of the object well (each of the 25 panels in Fig. 2A is for a specific background configuration; each gray point in the panels shows decoded banana position for a single presentation; the mean and standard deviation for each position - open circles and error bars - summarize our ability to predict the position of the banana from the activity of V4 neurons). The numbers at the upper left of each panel provide the correlation between the predicted and actual banana stimulus position (mean performance = 0.698).

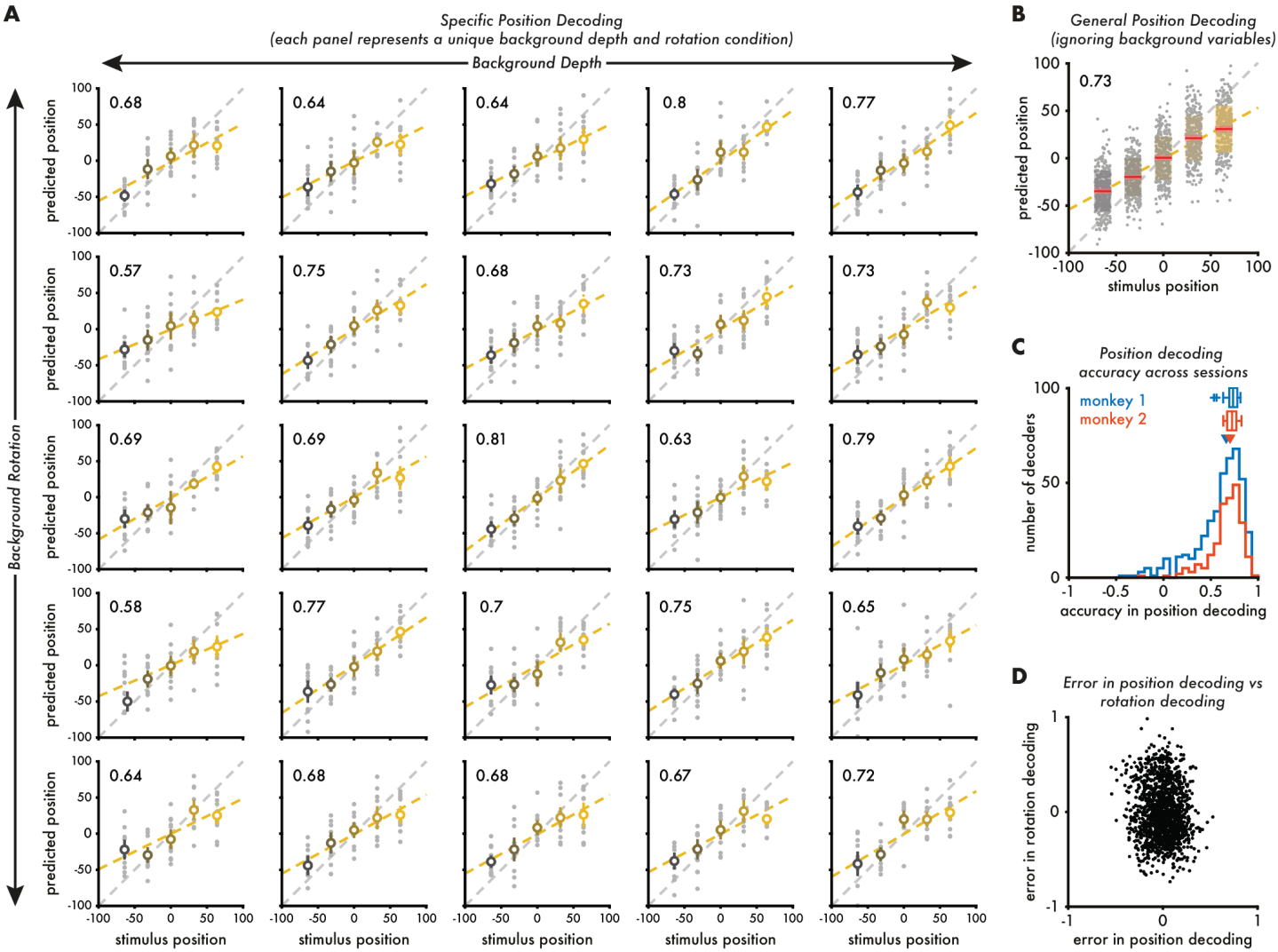

Figure 2: Object position decoding from V4 population responses is consistent across background variations.

A: We can linearly decode object position for each background stimulus (for the example session shown here). Each panel represents a unique configuration of background rotation and depth, with rows representing variations in rotation and columns representing variations in depth. Each gray point shows the decoded position for a single image presentation in this session. These points depict the actual object position (x-axis, in pixels relative to the center of the image) and the decoded position (y-axis) using a separate, cross-validated linear decoder for each unique background. The open circles represent the trial-averaged predicted position (vertical length is the standard deviation). The number in the top-left is the correlation between the actual and decoded positions and the yellow dashed line is a linear fit. Gray to yellow gradient is a redundant cue for stimulus position variation. The gray dashed line represents the identity.

B: Position decoding is largely consistent across background variations. This plot is in the same format as those in A. Here, a common decoder that ignores variations in the background and therefore incorporates all stimulus presentations is used. The data are the same as those shown in A. Compare with Supplementary Figure 2A and 2C for background rotation and depth decoding.

C: Distribution of specific decoder accuracies (correlation) across all sessions for each monkey (each session contributed 25 values to the histogram). Blue and red arrows represent the median accuracy (0.662 for monkey 1, 0.703 for monkey 2). The box plots above the histograms summarize general decoder accuracy across sessions for each monkey. The central line indicates the median (0.735 for monkey 1, 0.724 for monkey 2), box edges indicate 25 and 75 percentiles, whiskers indicate minimum and maximum values, and + symbols indicate outliers. Compare with Supplementary Figure 2B and 2D for background rotation and depth decoding.

D: Error in decoding object position (across background variations) for each trial compared with the error in decoding background rotation. See Supplementary Figure 2E for comparison with error in trial-wise background depth decoding.

V4 representations of stimulus position and background features are approximately orthogonal

Three lines of evidence support the view that the neural representation of the position of the central object (banana) in V4 is orthogonal to the representations of features of the background (depth and rotation of the leaves and branches) in our stimuli.

First, we compared our ability to decode stimulus position in each background (Fig. 2A) with our ability to decode the position of the banana across the entire stimulus set (Fig. 2B), where the variability in terms of background depth and rotation has the opportunity to intrude. The ability of a single decoder to read out banana position across all background variations is similar to that of the decoders that were optimized for each unique background stimulus (compare Fig. 2B with 2A) and is high across all sessions for two monkeys (Fig. 2C). We also found that our ability to decode background rotation (Supp Fig 2A, C) and depth (Supp Fig 2B, D) was similar using a single decoder for all stimuli and using a unique decoder for each combination of the other two features, suggesting that the same population of V4 neurons encodes all three axes of image variation well and orthogonally.

Second, we found that on a trial-by-trial basis, errors in the decoded estimates of banana position are not correlated with errors in decoding of background rotation and depth (Fig. 2D and Supp Fig. 2E). This lack of correlation also suggests that the representations of banana position are independent in V4 from representations of background rotation and depth.

Finally, if the representations of stimulus position and background parameters are orthogonal, then the decoders optimized for each unique stimulus (Fig. 2A) should be mutually aligned in neural population space. Put another way, if the representation of stimulus position is robust to variation in the background, this representation should vary along the same direction across backgrounds. To probe this, we calculated the line in neural population space that best explains population responses to each stimulus position for each background. These are depicted in Fig. 3A for each unique background condition (plotted for the first two principal components of the population neural responses for visualization purposes only; each point is a trial, each bright point is the average population response to a particular object position, and gray to yellow point colors represent the five object position values). The angle in the population space between the decoders for each unique background and the decoder for the background configuration whose decoder is shown in the center of 3A marked with $*$ (chosen as a reference simply to define the origin of the angular measure) is indicated in degrees. The distribution of angles for this example session (Fig. 3B) and across all sessions in both animals (Fig. 3C) is skewed toward much smaller angles than expected by chance – gray distributions in 3C depicting a median of ~90° for decoders trained on shuffled (randomizing trial labels within background configuration) responses to each unique background condition (labeled “shuffle”; dark gray) and angles between random vectors in a response space with the same dimensionality as the neural decoding space (labeled “random”; light gray).

Together, these recording results support the idea that the neural representation of stimulus position is orthogonal to the representations of background rotation and depth in V4.

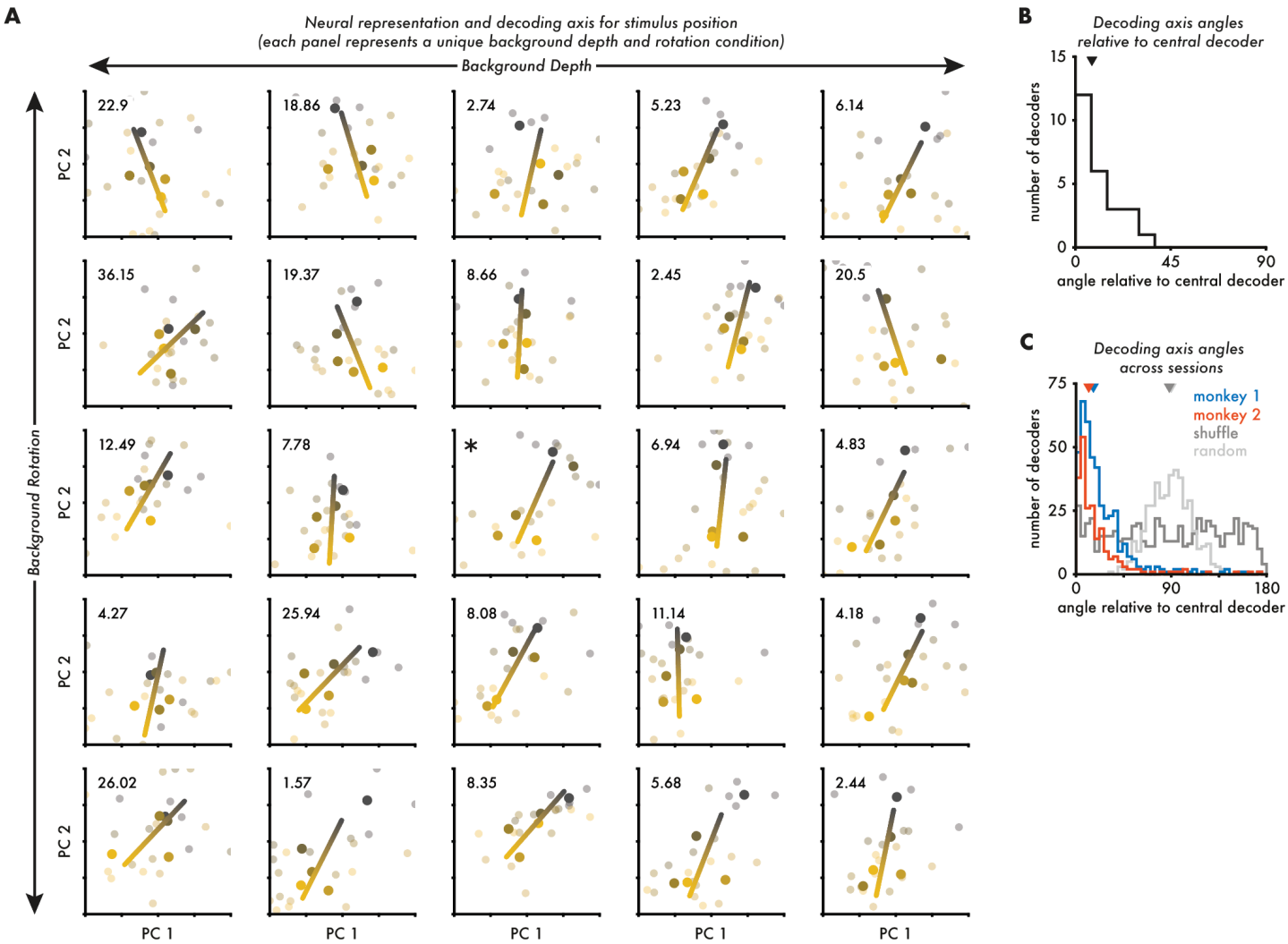

Figure 3: Object position axes across background variations are aligned with each other. Since object position decoding is tolerant to background variations, we tested whether the linear decoding axes for each background configuration were aligned by visualizing the decoders in the first two principal components of the neural response space. These dimensions were computed for the full set of neural responses obtained in each session.

A: As with Figure 2A, each panel represents a unique configuration of the background rotation and depth with rows representing variations in rotation and columns representing variations in depth. Each dim point represents a single image presentation, and bright points represent trial-averaged responses. Gray-to-yellow gradient represents monotonic variation in object position. A gradient line was fit to the responses for each background condition, shown here in two dimensions for illustration. The lines shown have been normalized to have the same length in the projected space shown. The text label at the top left represents the relative angle between each decoder and the central decoder (the middle background condition plot, marked with $*$) calculated in the full dimensional space of responses used for decoding.

B: Distribution of angles in A as a histogram. Arrow at the top represents the median angle for this session (7.78°).

C: Distribution of relative decoder angles across all object position decoders (like those in A) across sessions for both monkeys (blue and red distributions). Blue and red arrows represent the median of angles across sessions (16.4° for monkey 1, 12.07° for monkey 2). Dark gray distribution represents the angles of object position decoders after shuffling the position values for each trial (median 88.13°, shown as dark gray arrow). Light gray distribution represents the angles between randomly chosen vectors of the same dimensionality as the neural population space (median 89.99°, shown as light gray arrow).

Human subjects discriminate stimulus position robustly with respect to background variation

A prediction of our central hypothesis is that when the representations of two stimulus features are orthogonal in the brain, varying one should not impact the ability of subjects to discriminate the other. We tested this hypothesis by measuring the ability of human observers to discriminate the position of the central banana in our stimuli amid variation in the background rotation and depth.

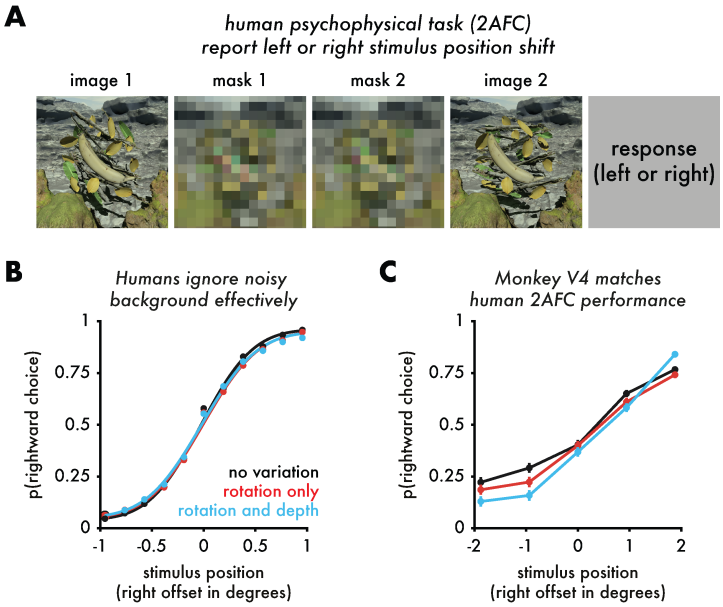

Figure 4: Human psychophysics experiments suggest that discrimination of object position is unaffected by variation in the stimulus background. Since object position representation in V4 neurons is robust to background variation, we tested whether changing background properties affects the decoding of object position in humans.
A: Human psychophysical task. Two images containing a banana were presented, with two masks in between. Participants were instructed to report whether the relative position of the banana in image 2 was left or right of that in image 1. In blocks, background rotation and/or depth were held constant or varied as described below.
B: Averaged (across participants, N = 10) psychometric functions for each background variation condition (individual participant performance shown in Supp. Fig. 3). Three background conditions were tested: black: no background variation between the two presentations of the banana on each trial; red: background rotation changed randomly across the two presentations of the banana, but background depth was held fixed; blue: both background rotation and depth were randomized across the two presentations of the banana. Across participants, object position change detection performance was not substantially different across the three background variation conditions.
C: To compare human behavior and monkey electrophysiology, we selected stimulus presentations in the monkey experiments to approximate the three background variation levels used in the human psychophysics experiment (see Methods for details of sample matching). We trained linear discriminants to separate trials into right or left position shift, for each background variation condition. During training, the trials with the banana in the central position were randomly assigned to be left or right. Classifier performance also did not differ substantially across the background variation conditions.

Human subjects viewed two images of the banana separated by two different masks (Fig. 4A) and reported whether the banana in the second image was positioned to the left or right of the banana in the first presentation. The offset between the two banana positions was varied systematically, to allow determination of discrimination threshold. Across blocks of trials, we varied the amount of within-trial image-to-image variability in the background objects across the two presentations of the banana. When there was background variation, intrusion of that variation on decoding of banana position would manifest itself as an elevated discrimination threshold if the representation of the banana position was not orthogonal to that of the background features[63,64]. However, consistent with the idea that the orthogonal representations of object position and background features that we found in the neural recordings enables background-independent perception, introducing variability into background did not significantly impact the position discrimination performance of human subjects (Fig. 4B and Supp Fig 3). To make a direct comparison between parameter decoding of neural representations and human psychophysical performance, we partitioned neural data into “no variation”, “rotation variation only”, and “depth

and rotation variation" groups and trained linear discriminants to classify left or right position difference between pairs of presentations (Fig. 4C). The cross-validated discrimination performance of these classifiers did not differ across the three background variation groups, as with the human psychophysical performance.

At least ten object and background features are represented approximately orthogonally in V4

To test the extent to which the orthogonality of representations of different features generalizes to other features of the banana and background in our stimuli, we measured V4 responses to a large image set where the color, luminance, position, rotation, and depth of both the background and object each took one of two values (this yields 2^{10} = 1,024 unique images; Fig. 5A). If any two parameters are encoded orthogonally in neural population space, then it should be possible to linearly decode those parameters successfully despite the variation in the others. Conversely, a decoder trained on one parameter should not provide information about the others. To test these predictions, we trained linear decoders for each of the object or background features and then tested our ability to decode each of the ten features with each decoder.

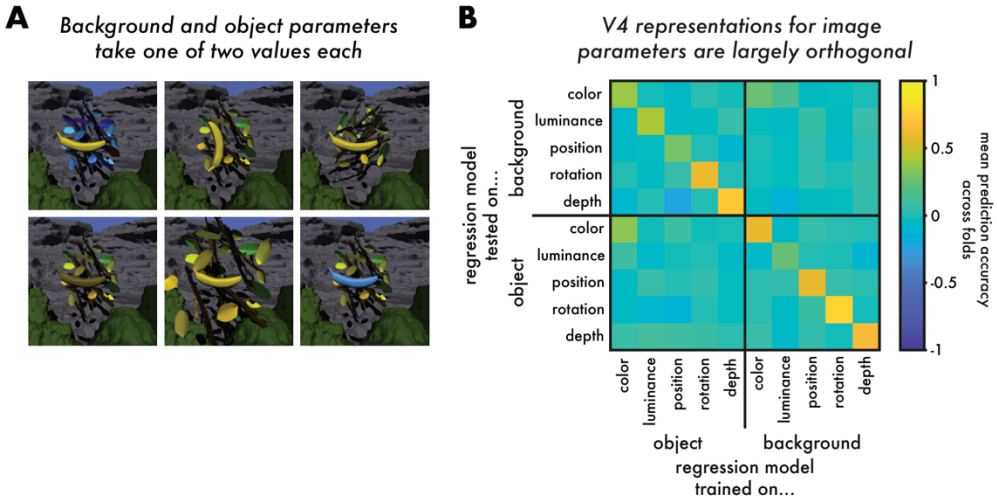

Figure 6: Orthogonal representations for variations in up to 10 object and background features. We generated a large image set where the color, luminance, position, rotation, and depth of both the background and object each took one of two values yielding 2^{10} = 1,024 images. We collected V4 population responses to these images as in Fig. 2C.
A: Example images illustrating object and background parameter variation.
B: If two features are encoded orthogonally (independently) in neural population space, then a decoder trained on one feature should not support decoding of the other feature. We trained linear decoders of V4 responses for each of the object or background features (x-axis) and tested the ability to decode each of the 10 features. The diagonal entries provide, for each feature the correlation between the decoded and actual feature parameter values for a decoder trained on that feature. Correlations obtained through cross-validation. Decoding performance was above chance (correlation of 0) for all features ($p < 10^{-80}$; t-test across folds). The off-diagonal values depict evaluate performance of a classifier trained on one feature (x-axis) for decoding another (y-axis). This cross-decoding performance was not distinguishable from chance except in the case of color of the object and background

Each of the ten features was encoded in the V4 population despite the variation in the other features, meaning that the correlation between the actual value of the feature parameter and the value predicted by a cross validated linear decoder was above chance (diagonals in Fig. 5B). In addition, the correlation between a given parameter and the value predicted by a decoder trained on a different parameter (off-diagonals in Fig. 5B) was indistinguishable from chance except in one case (the color of the central object and background objects). These observations suggest that a population of V4 neurons can encode a relatively large number of natural scene parameters

independently, enabling observers to avoid distraction by task-irrelevant stimulus features. The observation that there is an interaction between central and background objects presents an opportunity for future work to test the prediction that task-irrelevant variation in background object color should affect psychophysical discrimination of central object color, an outcome that would be consistent with the results of Singh et al[64].

Discussion

Using a combination of multi-neuron electrophysiology in monkeys and human psychophysics, we tested the hypothesis that features of irrelevant objects in naturalistic scenes will not interfere with the perception of target object features when their representations are orthogonal in visual cortex. We demonstrated that 1) in monkey area V4, the representation of object position is orthogonal to the representations of many irrelevant features of that object and the background, and 2) consistent with our hypothesis, the ability of human observers to judge object position was unaffected by the variations in the background stimulus that were shown neuronally to have orthogonal representations in monkey V4.

Relationship to the notion of untangling and representational geometry

The conditions under which objects can be disambiguated from neural population responses have been studied using the concept of *untangling*[59,65–67]. Untangling has been primarily discussed in the context of object classification. The hypothesis is that different objects can be appropriately classified (e.g. discriminating images of bananas from images of leaves) when the neural population representations of those objects are linearly separable in the face of irrelevant variations in the images (e.g. changes in position, orientation, size, or background). Support for this hypothesis comes from the observation that as one moves from early to late stages of the primate ventral visual stream, representations of different object categories become more linearly separable[60,66,68,69]. Progress has been made in understanding how the tuning functions and mixed selectivities of neurons support untangled population representations.[70–72]

The untangling framework has been extended to address the structure of neural populations that represent object categories more generally by characterizing the geometry of the high dimensional representational manifolds[27,73–77]. The capacity and dynamics of representational geometries in visual cortex correlate with classification behavior[38,66,78], in parietal and prefrontal cortices with perceptual decision making[79–82], and in motor cortex with control of muscle activity[83–86].

Here, we employ an analogous framework to explain the ability of observers to represent the continuous values taken on by lower-level visual features like the ones we studied. To connect the untangling idea as applied to object classification with the formulation here, note that the linear separability employed for object-class discrimination is effective when the effect of irrelevant image variations is orthogonal to the hyperplane that separates the classes in the neural population space. Here we use the same concept of orthogonality but apply it to linear decoding of feature parameter values rather than to linear separation of object classes. We link the neural orthogonality to behavioral performance by deploying a recently developed psychophysical paradigm[56,63,64] to quantify the degree of perceptual orthogonality between the same task-relevant and task-irrelevant stimulus features that we study neurally.

Other studies consistent with this line of thinking have also considered features and have demonstrated that neural responses to relevant and distracting features of simple stimuli are linearly separable in the brain areas (or analogous layers of deep network models of vision) that are thought to mediate that aspect of vision[59,68,75,87,88]. Indeed, a previous study in our lab also found a relationship between our ability to linearly decode visual information the activity of neural populations in monkeys and the ability of human observers to discriminate the same stimuli[56].

Opportunities from studying parameterizable naturalistic images

The present study extends the measurements of the relationship between the neural untangling of lower-level features and visually guided behavior with respect to features in naturalistic images. Our view is that the perception of object features in complex natural images provides increased power for testing the untangling hypothesis in the context of feature decoding. Unlike the case of simpler stimuli, the number of task-irrelevant features available for manipulation is larger and is likely to more fully challenge the coding capacity of neural populations whose representations are of limited dimensionality[74]. Furthermore, visual distractors (like variation in the background) heavily influence scene categorization performance in artificial stimuli but not natural stimuli, suggesting that orthogonal feature representations in natural stimuli are more resilient to noise[73,89]. Studying the relationship between neurons and visually guided behavior using parameterizable naturalistic images solves many of the challenges inherent in using simple artificial stimuli on the one hand or natural images on the other[1,2,90–93]. The graphics-generated stimuli we employ strike a balance between the experimental control available through parameterization and the ability to measure principles governing neural responses to and perception of features of natural images that are difficult or impossible to glean using artificial stimuli.

Opportunities from cross-species investigations of visual perception

Our results highlight the power of pairing neural population recordings in animals with behavior in humans for understanding the neural basis of visual perception. Although simultaneously recording neurons and behavior has many advantages, comparison with human performance provides assurance that the neural results obtained in an animal model generalize to humans. In addition, our approach links observations from the more peripheral visual field locations where for technical reasons the neural recordings are most often made, to the central visual field locations that are typically the focus of studies with human subjects.

Since the monkeys were performing a fixational task during the recordings, the neural responses we record seem more likely to be probing decoding of neural population activity that is stimulus driven, rather than activity that reflects the action of processes such as attention or motivation that have little to do with the stimuli themselves. Testing neural coding hypotheses (e.g. the untangling hypothesis) by making predictions about human behavior from neural responses in monkeys whose task is to fixate maximizes the likelihood that we are comparing behavior to stimulus-driven neural population responses.

Conclusion

Our results provide behavioral and neurophysiological evidence supporting the powerful untangling hypothesis, extend the study of untangling to representations of features of objects and

backgrounds, and demonstrate the value of parameterizable naturalistic images for studying the neural basis of visual perception. They also suggest a promising future of investigating the neural basis of perceptual and cognitive phenomena by leveraging the complementary strengths of multiple species.

Acknowledgements: We are grateful to K. McKracken for providing technical assistance, to Douglas Ruff, Cheng Xue, and Lily Kramer for comments on an earlier version of this manuscript and helpful comments and suggestions regarding data analysis. This work is supported by Eric and Wendy Schmidt AI in Science Postdoctoral Fellowship (to R.S.), the Simons Foundation (Simons Collaboration on the Global Brain award 542961SPI to M.R.C, postdoctoral fellowship to A.M.N.), the National Institutes of Health (awards R01EY022930, R01EY034723, and RF1NS121913 to M.R.C, 1K99NS118117-01 to A.M.N, K99EY035362 to R.S.)

Author Contributions: Conceptualization - A.M.N., M.R.C., D.H.B.; Methodology - R.S., A.M.N., M.R.C., D.H.B.; Software - R.S., A.M.N., D.H.B; Formal Analysis - R.S., A.M.N., C.M. M.R.C., D.H.B.; Investigation - R.S., A.M.N., C.M.; Data curation - R.S., A.M.N., C.M.; Writing – Original Draft - R.S., M.R.C., D.H.B. ; Writing – Review & Editing - R.S., M.R.C., D.H.B.; Visualization - R.S.; Supervision - M.R.C., D.H.B.; Project Administration - M.R.C., D.H.B. ; Funding acquisition - R.S., A.M.N., M.R.C., D.H.B.

Conflict of Interest: The authors declare no competing financial interests.

STAR ★ METHODS

KEY RESOURCES TABLE

RESOURCE AVAILABILITY

Lead Contact

Materials Availability

Data and Code Availability

EXPERIMENTAL MODEL AND SUBJECT DETAILS

Monkey electrophysiology

Human psychophysics

METHOD DETAILS

Monkey electrophysiology

Human psychophysics

QUANTIFICATION AND STATISTICAL ANALYSIS

Monkey electrophysiology

Human psychophysics

KEY RESOURCES TABLE

REAGENT or RESOURCE	SOURCE	IDENTIFIER
Experimental Models: Organisms/Strains		
Rhesus Macaques (Macaca mulatta)	University of Pittsburgh and Carnegie Mellon University	N/A
Software and Algorithms		
MATLAB	MathWorks	mathworks.com/products/matlab.html
Psychophysics Toolbox v3	[94]	psychtoolbox.org
Palamedes Toolbox	[95]	palamedestoolbox.org
ISET3D	[96,97]	github.com/ISET/iset3d
ISETBio	[98]	github.com/isetbio/isetbio
Blender	[99]	blender.org
MGL	[100]	http://justingardner.net/doku.php/mgl/overview
PBRT	[101,102]	github.com/mmp/pbrt-v3 github.com/scienstanford/pbrt-v3-spectral
Data Acquisition		
Blackrock 96-channel array	Blackrock Microsystems LLC Salt Lake City, UT 84108 USA	blackrockmicro.com
Blackrock CerePlex Data Acquisition System		
EyeLink 1000 Eye tracking system	SR Research Ottawa, Ontario, Canada., K2L 2B9	sr-research.com

RESOURCE AVAILABILITY

Lead Contact

Requests for resources should be directed to and will be fulfilled by the corresponding authors Marlene R. Cohen (marlenecohen@uchicago.edu), David H. Brainard (brainard@psych.upenn.edu).

Materials Availability

This study did not generate new unique reagents.

Data and Code Availability

The data and code that generate the figures in this study have been deposited in a public Github repository https://github.com/ramanujansrinath/UntanglingBananas. MATLAB code for creating and displaying the images for human psychophysical experiments, as well as analyzing the raw data from these experiments, can be found at https://github.com/AmyMNi/NaturalImageThresholds. Request for further information should be directed to and will be fulfilled by the corresponding author David H. Brainard (brainard@psych.upenn.edu) in consultation with the other authors.

EXPERIMENTAL MODEL AND SUBJECT DETAILS

Monkey electrophysiology

Two adult male rhesus monkeys (Macaca mulatta, 10 and 11 kg) were implanted with titanium head posts before behavioral training. Subsequently, multielectrode arrays were implanted in cortical area V4 identified by visualizing the sulci and using stereotactic coordinates. All animal procedures were approved by the Institutional Animal Care and Use Committees of the University of Pittsburgh and Carnegie Mellon University.

Human Psychophysics

This study was preregistered at ClinicalTrials.gov, NCT number NCT05004649, https://clinicaltrials.gov/ct2/show/NCT05004649. The experimental protocols were approved by the University of Pennsylvania Institutional Review Board. Participants were invited to volunteer to participate in this study. Participants provided informed consent and filled out a lab participant survey. We also screened for visual acuity using a Snellen eye chart and for color deficiencies using the Ishihara plate test. Participants were excluded prior to the experiment if their best-corrected visual acuity was worse than 20/40 in either eye or if they made any errors on the Ishihara plate test.

Participants were excluded after the conclusion of their first session if their horizontal position discrimination threshold in the no variation condition (see description of conditions below) was higher than 0.6 degrees of visual angle, and participants excluded at this point did not participate in any further experimental sessions.

METHOD DETAILS

Image Generation (for both human psychophysics and monkey electrophysiology)

All the stimuli were variants of the same natural visual scene: a square image with a central object (a banana) presented on an approximately circular array of overlapping background objects (made up of overlapping branches and leaves). The central object and/or the background objects changed in horizontal position, rotation, and/or depth across different stimuli. In the larger set of stimuli (detailed below) the luminance and color of the central and background objects also changed. The central object and background objects are presented in the context of other objects (a rock ledge, a skyline, and three moss-covered stumps) that remain unchanged across all stimulus conditions. This natural visual scene was created using Blender, an open-source 3D creation suite (https://www.blender.org, Version 2.81a). The object and background parameters were varied using ISET3d, an open-source software package (https://github.com/ISET/iset3d) that works with a modified version of PBRT (https://github.com/scienstanford/pbrt-v3-spectral; unmodified version at https://github.com/mmp/pbrt-v3).

The images created using ISET3d were converted to RGB images using custom software (Natural Image Thresholds; https://github.com/AmyMNi/NaturalImageThresholds) written using MATLAB (MathWorks; Natick, MA) and based on the software package Virtual World Color Constancy (github.com/BrainardLab/VirtualWorldColorConstancy). Natural Image Thresholds is dependent on routines from the Psychophysics Toolbox (http://psychtoolbox.org), ISET3d (https://github.com/ISET/iset3d), ISETBio (http://github.com/isetbio/isetbio), PBRT (https://github.com/scienstanford/pbrt-v3-spectral; unmodified version at https://github.com/mmp/pbrt-v3), and the Palemedes Toolbox (palamedestoolbox.org).

To convert a hyperspectral image created using ISET3d to an RGB image for presentation on the calibrated monitor, the hyperspectral image data were first used to compute LMS cone excitations. The LMS cone excitations were converted to a metameric rendered image in the RGB color space of the monitor, based on the monitor calibration data. A scale factor was applied to this image so that its maximum RGB value was 1 and the image was then gamma corrected, again using monitor calibration data. This process was completed separately for the two different monitors used, one for the psychophysics and one for the neurophyisology.

Monkey electrophysiology

<u>Array implantation, task parameters</u>

Both animals were implanted with titanium headposts prior to behavioral training. After training, microelectrode arrays were implanted in area V4 (96 recording sites; Blackrock Microsystems). Array placement was guided by stereotactic coordinates and visual inspection of the sulci and gyri. The monkeys were trained to perform a fixation task along with other behavioral tasks that were not relevant to this study. The stimulus images used in this study were not displayed outside of the context of this task. The monkeys fixated a central spot for a pre-stimulus blank period of 150-400ms followed by stimulus presentations (200-250ms) interleaved with blank intervals (200-250ms). The stimuli were presented one at a time at a peripheral location that overlapped the receptive fields of the recorded neurons. In each trial, 6-8 stimuli were presented, after which the monkey received a liquid reward for having maintained fixation on the central spot until the end of the stimulus presentations. If the monkey broke fixation before the end of the stimulus presentations, the trial was terminated. The intertrial interval was at least 500ms. The stimuli were presented pseudorandomly.

The visual stimuli were presented on a calibrated (X-Rite calibrator) 24” ViewPixx LCD monitor (1920 x 1080 pixels; 120 Hz refresh rate) placed 54 cm (monkey 1) or 56 cm (monkey 2) from the monkey, using custom software written in MATLAB (Psychophysics Toolbox; Brainard, 1997; Pelli, 1997). Eye position was monitored using an infrared eye tracker (Eyelink 1000; SR Research). Eye position (1000 samples/s), neuronal activity (30,000 samples/s) and the signal from a photodiode was recorded to align neuronal responses to stimulus presentation times (30,000 samples/s) using Blackrock CerePlex hardware.

Neural responses

The filtered electrical activity (bandpass 250-5000Hz) was thresholded at 2-3% RMS value for each recording site and the threshold crossing timestamps were saved (along with the raw electrical signal, waveforms at each crossing, and other signals). Spikes were not sorted for these experiments and ‘unit’ refers to the multiunit activity at each recording electrode. The stimulus-evoked firing rate of each V4 unit was calculated based on the spike count responses between 50-250ms after stimulus onset, to account for V4 response latency. The baseline firing rates were calculated based on the spike count responses in the 100ms time-period prior to the onset of the stimulus.

Neuron exclusion

For each experimental session, for each unit, the average stimulus-evoked responses across all stimuli were compared with its average baseline activity. The unit was included in further analyses if the average evoked activity was at least 1.1x the baseline activity. This lenient inclusion criterion was chosen because, for the chosen experimental design and stimuli, dimensionality reduced decoding analyses are resilient to noise and benefit from information distributed across many neurons. Each recording experiment yielded data from 90-95 units (mean 94.1).

Receptive Field Mapping

A set of 2D closed contours, 3D solid objects, and black-and-white Gabor images were flashed with the same timing as described above in the lower left quadrant of the screen. The positions and sizes were chosen manually across several experiments to home in on the receptive fields of each V4 recording site. Typically, a grid of 5x5 positions and 2 image sizes were chosen such that the images overlapped partially. The spikes were counted within a 50-250ms window after stimulus onset and a RF heat map was constructed for each site. The center of mass of this heat map was chosen as the center of the RF and an ellipse was fit to circumscribe the central two standard deviations. This resulted in centers and extents of the RF of each recording site. The naturalistic image sets for the experiments described below were scaled such that the circular aperture within which the background objects were contained fully overlapped the population RF. This necessitated that the image boundary exceeded the RF of some neurons but the image information outside of the circular aperture was held constant across images.

Experiment 1: Effect of task-irrelevant stimulus changes on the ability of V4 neurons to encode a feature of interest about the central object

The first goal of the electrophysiology experiments was to determine if the information about the chosen parameter of the central object (banana position) interferes with information about distracting parameters (background object rotation and depth). To do this, we systematically varied the horizontal position of the object and the background parameters in an uncorrelated

fashion. The values and ranges of the object and background parameters were customized for each monkey such that there was a differential response to each condition on average across all other conditions i.e., a 3-way ANOVA for object position and the two background conditions all had a significant main effect ($p<0.01$). Five values of object position, background depth, and background rotation were chosen and permuted yielding 125 image stimuli. Further details of stimuli can be found in Figure 1, Supplemental Figure 1, and the associated code and data repositories.

The data were collected in 26 recording experiments (17 sessions across 11 days from monkey 1, 9 sessions across 8 days from monkey 2). Recording experiments with fewer than 3 repetitions per stimulus image were excluded. Each stimulus was therefore presented between 3 and 16 times yielding between 381-2084 presentations (mean 831).

Experiment 2: Relationships between multiple feature dimensions

The second goal of the monkey electrophysiology was to determine different visual features are encoded orthogonally in neuronal population responses. We therefore measured responses to stimuli that varied many features of the central object (banana), including its horizonal position, depth, orientation, and two surface parameters (color and luminance). We also varied the same five features of the background objects (branches and leaves) in an independent way. We used two values of each of the ten features, which we chose to make the ten features equally decodable by the population of V4 neurons (see Figure 5). We therefore measured responses to five repetitions of each of 2^{10}=1024 stimuli. Each stimulus image was repeated between two to three times. Because of the large dataset required for this experiment, the data analyzed in Figure 5 were collected from one session from monkey 1.

Human psychophysics

Apparatus

A calibrated LCD color monitor (27-inch NEC MultiSync PA271Q QHD Color Critical Desktop W-LED Monitor with SpectraView Engine; NEC Display Solutions) displayed the stimuli in an otherwise dark room, after participants dark-adapted in the experimental room for a minimum of 5 minutes. The monitor was driven at a pixel resolution of 1920 x 1080, with a refresh rate of 60 Hz and with 8-bit resolution for each RGB channel. The host computer for this monitor was an Apple Macintosh with an Intel Core i7 processor. The head position of each participant was stabilized using a chin cup (Headspot, UHCOTech, Houston, TX). The participant's eyes were centered horizontally and vertically with respect to the monitor, which was 75 cm from the participant's eyes. The participant indicated their responses using a Logitech F310 gamepad controller.

Stimulus parameters

The entire image subtended 8 degrees in both width and height, the central object subtended ~4 degrees in the longest dimension, and the circular array of background objects (branches and leaves) subtended ~5 degrees of visual angle. The images were created using ISET3d at a resolution of 1920 x 1920 with 100 samples per pixel, at 31 equally spaced wavelengths between 400 nm and 700 nm.

Psychophysical task

The psychophysical task was a two-interval forced choice task with one stimulus per interval. Each stimulus interval had a duration of 250 ms. Stimuli were presented at the center of the monitor. Between the two stimulus intervals, two masks were shown in succession at the center of the monitor (Figure 5). Each mask was be presented for a duration of 400 ms, for a total interstimulus interval of 800 ms (see Session organization below for mask details). Display times are approximate as the actual display times were quantized by the hardware to integer multiples of the 16.67 ms frame rate.

The task of the participant was to determine whether, compared to the central object presented in the first interval, the central object presented in the second interval was to the left or to the right. Following the two intervals, the participant had an unlimited amount of time to press one of two response buttons on a gamepad to indicate their choice. Feedback was provided via the auditory tones. Trials were be separated by an intertrial interval of approximately 1 second.

The experimental programs can be found in the custom software package Natural Image Thresholds (https://github.com/AmyMNi/NaturalImageThresholds). They were written in MATLAB (MathWorks; Natick, MA) and were based on the software package Virtual World Color Constancy (github.com/BrainardLab/VirtualWorldColorConstancy). They rely on routines from the Psychophysics Toolbox (http://psychtoolbox.org) and mgl (http://justingardner.net/doku.php/mgl/overview).

Session organization

The first session experimental session for each participant included participant enrollment procedures (informed consent, vision tests, etc.; see Participants above for details) as well as familiarization trials (see next paragraph) and lasted one and a half hours. The additional experimental sessions lasted approximately one hour each.

For the first session only, the participant began with 30 familiarization trials. The familiarization trials comprised, in order: 10 randomly selected easy trials (the largest position-change comparisons), 10 randomly selected medium-difficulty trials (the 4th and 5th largest position-change comparisons), and 10 randomly selected trials from all possible position-change comparisons. The familiarization trials did not include any task-irrelevant variability and data from these trials was not saved.

In each session, there were two reference positions for the banana, and for each reference position there were 11 comparison positions: five comparison positions in the positive horizontal direction, five comparison positions in the negative horizontal direction, and a comparison position of 0 indicating no change. On each trial, one interval contained one of the two reference stimuli and the other interval will contain one of that reference stimulus's comparison stimuli. The order in which these two stimuli were presented within a trial was selected randomly per trial.

A block of trials consisted of presentation of the 11 comparison positions for each of the two reference positions for a total of 22 trials per block. The trials within a block were run in randomized order. Each was completed before the next block began. Each block was repeated 7 times in a run of trials, for a total of 154 trials per run.

Within each run of 154 trials, a single background variation condition was studied. There were three such conditions, as described in more detail below – "no variation", "rotation only", and "rotation and depth". Two runs for each of the three conditions was completed in each

experimental session, and except as noted in the results, each subject completed 6 sessions. The six runs were conducted in random order within each session, and each run was separated by a break that lasted at least one minute and during which the participant was encouraged to stand or stretch as needed. After a minimum of one minute, the next run was initiated when the participant was ready.

Additionally, each session began with four practice trials (including in the first experimental session, where these practice trials were preceded by the familiarization trials as described). Each run after the first also started with one practice trial. The practice trials were all easy trials as described above and not include any task-irrelevant variability. The data from the practice trials was be saved. The maximum variation in background features was matched to the maximum variation in the neurophysiology experiments but sampled more finely as described for each of the variation blocks below.

For the “no variation” condition, there were not any changes to the background objects (the branches and leaves). This run determines the participant’s threshold for discriminating the horizontal position of the central object without any task-irrelevant stimulus variation.

The “rotation only” run introduced task-irrelevant variability single task-irrelevant feature: rotation. For each trial, a single rotation amount was drawn randomly from a pool of 51 rotations, and the background objects (leaves and sticks) in the stimulus were all rotated by that amount around their own centers. The rotation was drawn separately (randomly with replacement) for each of the two stimuli presented on a trial (the reference position stimulus and the comparison position stimulus). Thus subjects had to judge the position of the central object across a change in the background, so that any effect of background variation on the positional representation of the central object would be expected to elevate threshold. The pool of 51 rotations comprised: a rotation of zero (no change to the background objects), 25 equally spaced rotations in the clockwise direction in 2-degree intervals, and 25 equally spaced rotation amounts in the counterclockwise direction in 2-degree intervals.

“Rotation and depth” runs had variation in two task-irrelevant features: rotation and depth of the background objects. For this run, there was a pool of 51 rotations, but along with the rotation of the background objects, these objects also varied in depth. There were 51 possible depth amounts (one depth amount of zero, 25 equally spaced depth amounts in the positive depth direction, and 25 equally spaced depth amounts in the negative direction; depth amounts ranged from -500 mm to 500 mm in the rendering scene space). One of the of images was a rotation of zero and a depth amount of zero. For the remaining 50 images in the pool, each of the remaining 50 rotation amounts was randomly assigned (without replacement) to one of the remaining 50 depth amounts. The same depth shift was applied to each of the background objects. From this pool of 51 images, a single image was randomly drawn (with replacement) for each of the two stimuli presented in the trial.

Finally, as noted above (see Psychophysical task), two masks were shown per trial during the interstimulus interval. All masks across all background variation conditions were created from the same distribution of stimuli (stimuli with “no variation”, thus containing no task-irrelevant noise). To create each of the two masks, first the central object positions in the first and second intervals of the trial were be determined. The two stimuli with that matched the central object positions in the first and second intervals were then used to create the trial masks. For each of these two stimuli, the average intensity was calculated in each RGB channel per 16 x 16 block of

603 the stimulus. Next, each 16 x 16 block of a mask was randomly drawn from the mask
604 corresponding to the two stimuli. Thus, the two masks shown per trial were each a random mixture
605 of 16 x 16 blocks from stimuli with the two central object positions for that trial.

606

607 ***QUANTIFICATION AND STATISTICAL ANALYSIS***

608 *Monkey electrophysiology*

609 Cross-validated Parameter Decoding (Figure 2)

610 First, the response matrix (multiunit spike rates for each site for each image stimulus
611 presentation) was reduced to 10 dimensions of activity. This ensured sufficient dimensionality for
612 the decoding of object and background parameters and explained between 87.8% and 94.8%
613 (mean 91.2%) of the variance across stimulus responses. (Parameter decoding without
614 dimensionality reduction produced qualitatively similar results.) Then, for each background
615 condition (unique combination of background rotation and depth – or "specific decoding"), the
616 object position in each presentation/trial was decoded from neural responses by learning
617 regression weights from all other trials (leave-one-out cross-validation). The same procedure was
618 repeated for "general decoding" where the background parameters were ignored (Figure 2B).
619 Decoding accuracy was defined as the correlation between the actual values and the decoded
620 values. Perfect decoding would result in an accuracy of 1 and chance decoding in an accuracy of
621 0. We did not encounter decoding accuracies below 0. Error in decoding was defined as the
622 difference between the predicted object position and the actual position (Figure 2D). The same
623 procedure for specific and general decoding was repeated for each of the two background
624 conditions as well (Supplementary Figure 2).

625 Angle calculation (Figure 3)

626 To calculate the angle between the specific decoders, an n-dimensional line was fit to the
627 dimensionality reduced responses and the unit vector was found. The angle between each
628 specific decoder and the decoder for the central condition was calculated as the arc-cos of the dot
629 product of the two unit vectors.

630 Linear discriminant analysis and comparison with human psychophysics (Figure 4)

631 To directly compare human psychophysics discrimination accuracy with decoding results,
632 we matched the three blocked conditions – no background variation, rotation only, and rotation
633 and depth variation – by subsampling trials from the 5x5x5 stimulus set from experiment 1. For the
634 three conditions, we either found all pairs of trials, pairs of trials that varied in rotation only (by
635 holding background depth at the central value), or pairs of trials that varied in depth only (by
636 holding background rotation at the central value). Then, for 200 folds, we sampled a maximum of
637 500 pairs of trials and depending upon the object position on those trials, we assigned a left or
638 right choice. If the positions were identical, we randomly assigned the choice for that pair. We then
639 collated the responses across the pairs of trials and a fit linear discriminant in a leave-one-out
640 fashion to predict the correct choice. The classification prediction accuracy for each of the three
641 blocked conditions was calculated independently.

642 Cross-decoding analysis (Figure 5)

643 For experiment 2, even though only two values were chosen for each of the five object and
644 five background parameters, linear regression was chosen to instead of classification using

discriminant analysis for comparison with decoding analyses in the previous experiment. Even though each stimulus image was only repeated 2-3 times, since each parameter could take one of two values each, all unique pairs of images would be informative about at least one parameter change. To enable cross-decoding, we altered the cross-validation procedure. For each parameter pair, for each of 100 folds, we randomly split all image presentations evenly into training and testing sets (uneven splits also produced qualitatively similar results). We then trained a linear regression model for one parameter using the training trials and used it to predict the values of the other parameter for the held-out testing trials. The decoding accuracy was calculated as the average correlation across folds between the actual and decoded parameter values. Since each parameter decoder was trained while ignoring all other parameter variations, the diagonals in Figure 5B are akin to the general decoder accuracy for those parameters, and the off diagonals correspond to how well those general decoders are aligned to the representations of the other parameters. The diagonal correlations were all significantly above 0 ($p < 10^{-80}$; t-test across folds) and none of the off-diagonal correlations were except the cross-decoding of background and object color.

Human psychophysics

Per session, the participant's threshold for discriminating object position was measured for each background variation condition. First, for each comparison position, the proportion of trials on which the participant responded that the comparison stimulus was located to the right of the reference stimulus was calculated. Next, the proportion the comparison was chosen as rightwards was fit with a cumulative normal function using the Palamedes Toolbox (http://www.palamedestoolbox.org). To estimate all four parameters of the psychometric function (threshold, slope, lapse rate, and guess rate), the lapse rate was constrained to be equal to the guess rate and to be in the range [0, 0.05] and the maximum likelihood fit determined. Threshold was calculated as the difference between the stimulus levels at performances (proportion the comparison was chosen as rightwards) equal to 0.7602 and 0.5 as determined by the cumulative normal fit.

Supplementary Materials

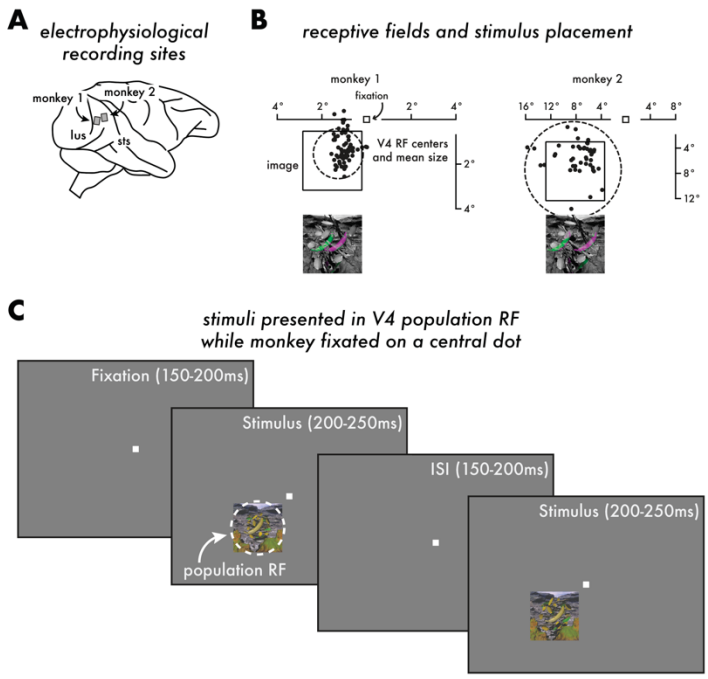

Supplementary Figure 1: Recording locations, stimulus positions, and behavioral task for monkeys.
A: Multielectrode arrays (96 channels each) were chronically implanted in V4 of two monkeys.
B: The receptive fields of the recorded multiunits were mapped using Gabor and two-dimensional shape stimuli. The estimated receptive field (RF) center of each visually responsive multiunit is depicted by a black point. The mean size of the RF for each population is depicted by the dashed circle. The black square indicates the position of the image on the screen. The size and position of the images for each session were chosen such that all the variations in stimulus position and background depth were within the estimated RF of the recorded V4 population. The variation in object position is indicated by the false color image in each panel. **C:** While monkeys fixated a central dot, stimuli were flashed on (200-250 ms) and off (150-200 ms) up to eight times before the monkey received a juice reward. Each of the 125 images was repeated between 8-10 times in every session. Electrophysiological recordings were collected using multielectrode arrays implanted in V4. Receptive fields (RFs) were mapped in an independent experiment using Gabor and 2D shape stimuli. Images were placed such that the variation in the central object (the banana) and background overlapped a large majority of RFs (see Supplementary Figure 1).

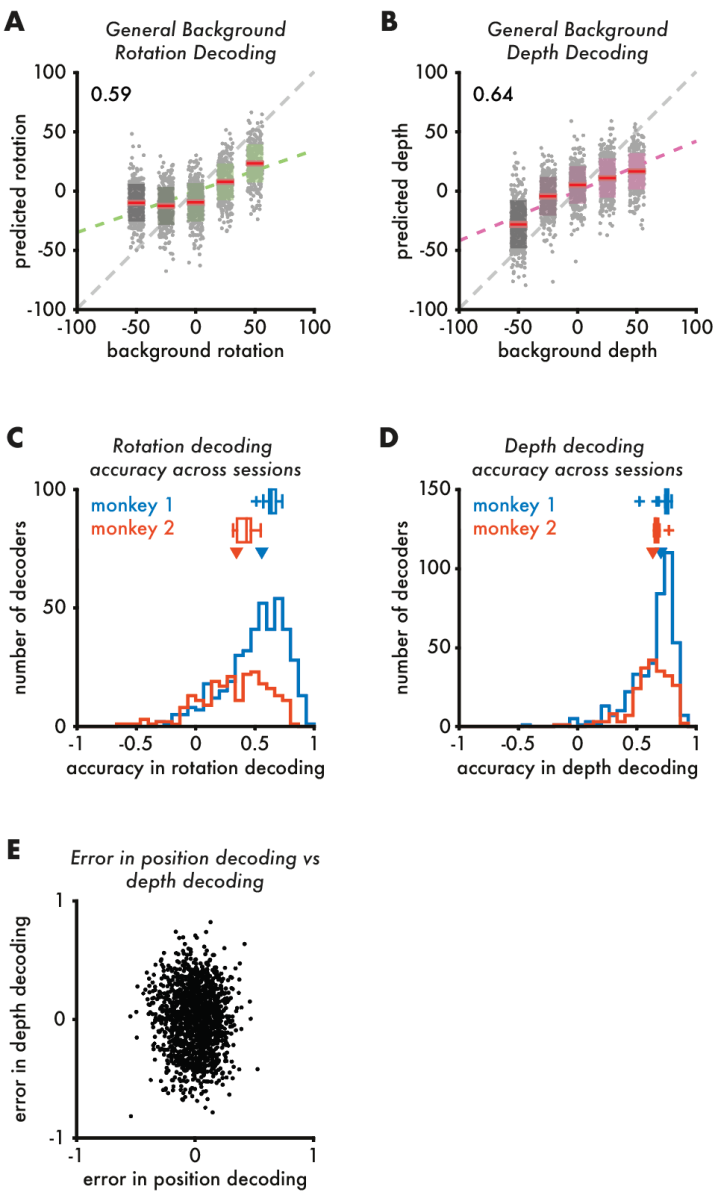

Supplementary Figure 2: Background depth and rotation can also be decoded well from V4 population responses. Compare with Figure 2.
A: Same as Figure 2B but for background rotation. Here, a general linear decoder was used to estimate the background rotation value in the face of variation in background depth and banana position.
B: Same as Figure 2B but for background depth. Here, a general linear decoder was used to estimate the background depth value was decoded in the face of variation in background rotation and object position.
C: Same as Figure 2C for specific background rotation decoding (each session contributes 25 values to the distribution). Here, the background rotation value was decoded while ignoring the other parameter variations across images. Arrows represent median decoding accuracy (0.558 for monkey 1, 0.344 for monkey 2). Box plots above the histograms show distribution of general decoder performance.
D: Same as Figure 2C for specific background depth decoding (each session contributes 25 values to the distribution). Arrows represent median decoding accuracy (0.703 for monkey 1, 0.634 for monkey 2). Box plots above the histograms show distribution of general decoder performance.
E: Comparison of errors for general decoding of object position and general decoding of background depth across trials. Compare with Figure 2D.

Supplementary Figure 3: Psychometric functions for object position discrimination for each participant.

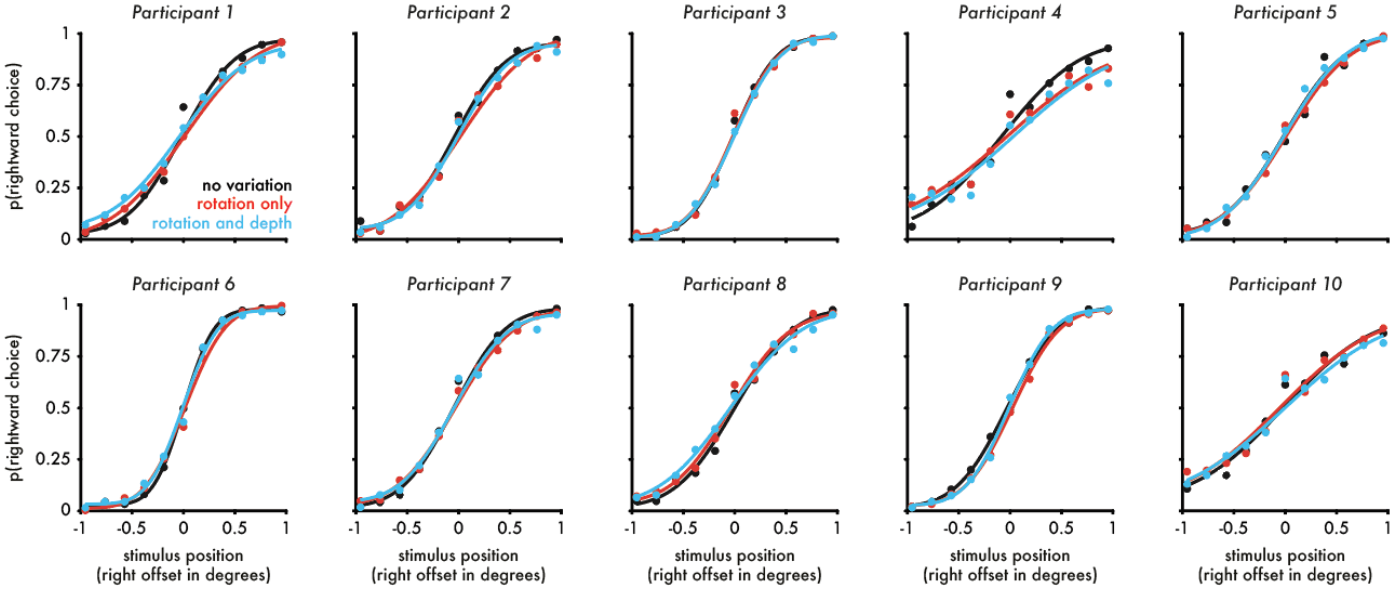

References

1. Martinez-Garcia, M., Bertalmío, M., and Malo, J. (2019). In Praise of Artifice Reloaded: Caution With Natural Image Databases in Modeling Vision. Front. Neurosci. *13*, 8. 10.3389/fnins.2019.00008.

2. Rust, N.C., and Movshon, J.A. (2005). In praise of artifice. Nat. Neurosci. *8*, 1647–1650. 10.1038/nn1606.

3. Pasupathy, A., and Connor, C.E. (2002). Population coding of shape in area V4. Nat. Neurosci. *5*, 1332–1338. 10.1038/972.

4. Gallant, J.L., Braun, J., and Essen, D.V. (1993). Selectivity for polar, hyperbolic, and Cartesian gratings in macaque visual cortex. Science *259*, 100–103. 10.1126/science.8418487.

5. Leopold, D.A., and Logothetis, N.K. (1996). Activity changes in early visual cortex reflect monkeys' percepts during binocular rivalry. Nature *379*, 549–553. 10.1038/379549a0.

6. Peterhans, E., and Heydt, R. von der (1991). Subjective contours - bridging the gap between psychophysics and physiology. Trends Neurosci. *14*, 112–119. 10.1016/0166-2236(91)90072-3.

7. von der Heydt, R., Peterhans, E., and Baumgartner, G. (1984). Illusory Contours and Cortical Neuron Responses. Science *224*, 1260–1262. 10.1126/science.6539501.

8. Snow, J.C., and Culham, J.C. (2021). The Treachery of Images: How Realism Influences Brain and Behavior. Trends Cogn. Sci. *25*, 506–519. 10.1016/j.tics.2021.02.008.

9. Peters, B., and Kriegeskorte, N. (2021). Capturing the objects of vision with neural networks. Nat. Hum. Behav. *5*, 1127–1144. 10.1038/s41562-021-01194-6.

10. Ruff, D.A., and Cohen, M.R. (2016). Stimulus Dependence of Correlated Variability across Cortical Areas. J. Neurosci. *36*, 7546–7556. 10.1523/JNEUROSCI.0504-16.2016.

11. Cohen, M.R., and Maunsell, J.H.R. (2009). Attention improves performance primarily by reducing interneuronal correlations. Nat. Neurosci. *12*, 1594–1600. 10.1038/nn.2439.

12. Ruff, D.A., Ni, A.M., and Cohen, M.R. (2018). Cognition as a Window into Neuronal Population Space. Annu. Rev. Neurosci. *41*, 77–97. 10.1146/annurev-neuro-080317-061936.

13. Srinath, R., Ruff, D.A., and Cohen, M.R. (2021). Attention improves information flow between neuronal populations without changing the communication subspace. Curr. Biol. *31*, 5299-5313.e4. 10.1016/j.cub.2021.09.076.

14. Ruff, D.A., and Cohen, M.R. (2019). Simultaneous multi-area recordings suggest that attention improves performance by reshaping stimulus representations. Nat. Neurosci. *22*, 1669–1676. 10.1038/s41593-019-0477-1.

15. Ni, A.M., Ruff, D.A., Alberts, J.J., Symmonds, J., and Cohen, M.R. (2018). Learning and attention reveal a general relationship between population activity and behavior. Science *359*, 463–465. 10.1126/science.aao0284.

16. Ni, A.M., Bowes, B.S., Ruff, D.A., and Cohen, M.R. (2022). Methylphenidate as a causal test of translational and basic neural coding hypotheses. Proc. Natl. Acad. Sci. U. S. A. *119*, e2120529119. 10.1073/pnas.2120529119.

17. Kriegeskorte, N., and Douglas, P.K. (2019). Interpreting encoding and decoding models. Curr. Opin. Neurobiol. *55*, 167–179. 10.1016/j.conb.2019.04.002.

18. Simoncelli, E.P., and Olshausen, B.A. (2001). Natural Image Statistics and Neural Representation. Annu. Rev. Neurosci. *24*, 1193–1216. 10.1146/annurev.neuro.24.1.1193.

19. Iyer, A., and Burge, J. (2019). The statistics of how natural images drive the responses of neurons. J. Vis. *19*, 4. 10.1167/19.13.4.

20. Haxby, J.V., Gobbini, M.I., Furey, M.L., Ishai, A., Schouten, J.L., and Pietrini, P. (2001). Distributed and Overlapping Representations of Faces and Objects in Ventral Temporal Cortex. Science *293*, 2425–2430. 10.1126/science.1063736.

21. Chung, S., Lee, D.D., and Sompolinsky, H. (2016). Linear readout of object manifolds. Phys. Rev. E *93*, 060301. 10.1103/PhysRevE.93.060301.

22. Kriegeskorte, N. (2011). Pattern-information analysis: From stimulus decoding to computational-model testing. NeuroImage *56*, 411–421. 10.1016/j.neuroimage.2011.01.061.

23. Kohn, A., Jasper, A.I., Semedo, J.D., Gokcen, E., Machens, C.K., and Yu, B.M. (2020). Principles of Corticocortical Communication: Proposed Schemes and Design Considerations. Trends Neurosci. *43*, 725–737. 10.1016/j.tins.2020.07.001.

24. Vyas, S., Golub, M.D., Sussillo, D., and Shenoy, K.V. (2020). Computation Through Neural Population Dynamics. Annu. Rev. Neurosci. *43*, 249–275. 10.1146/annurev-neuro-092619-094115.

25. Okazawa, G., Hatch, C.E., Mancoo, A., Machens, C.K., and Kiani, R. (2021). Representational geometry of perceptual decisions in the monkey parietal cortex. Cell *184*, 3748-3761.e18. 10.1016/j.cell.2021.05.022.

26. Misaki, M., Kim, Y., Bandettini, P.A., and Kriegeskorte, N. (2010). Comparison of multivariate classifiers and response normalizations for pattern-information fMRI. NeuroImage *53*, 103–118. 10.1016/j.neuroimage.2010.05.051.

27. Saxena, S., and Cunningham, J.P. (2019). Towards the neural population doctrine. Curr. Opin. Neurobiol. *55*, 103–111. 10.1016/j.conb.2019.02.002.

28. Kaufman, M.T., Churchland, M.M., Ryu, S.I., and Shenoy, K.V. (2014). Cortical activity in the null space: permitting preparation without movement. Nat. Neurosci. *17*, 440–448. 10.1038/nn.3643.

29. Semedo, J.D., Zandvakili, A., Machens, C.K., Yu, B.M., and Kohn, A. (2019). Cortical Areas Interact through a Communication Subspace. Neuron *102*, 249-259.e4. 10.1016/j.neuron.2019.01.026.

30. Ruff, D.A., and Cohen, M.R. (2019). Simultaneous multi-area recordings suggest that attention improves performance by reshaping stimulus representations. Nat. Neurosci. *22*, 1669–1676. 10.1038/s41593-019-0477-1.

31. Kiani, R., Esteky, H., Mirpour, K., and Tanaka, K. (2007). Object category structure in response patterns of neuronal population in monkey inferior temporal cortex. J. Neurophysiol. *97*, 4296–4309. 10.1152/jn.00024.2007.

32. Cunningham, J.P., and Yu, B.M. (2014). Dimensionality reduction for large-scale neural recordings. Nat. Neurosci. *17*, 1500–1509. 10.1038/nn.3776.

33. Kiani, R., Cueva, C.J., Reppas, J.B., Peixoto, D., Ryu, S.I., and Newsome, W.T. (2015). Natural Grouping of Neural Responses Reveals Spatially Segregated Clusters in Prearcuate Cortex. Neuron *85*, 1359–1373. 10.1016/j.neuron.2015.02.014.

34. Cowley, B.R., Smith, M.A., Kohn, A., and Yu, B.M. (2016). Stimulus-Driven Population Activity Patterns in Macaque Primary Visual Cortex. PLoS Comput. Biol. *12*, e1005185. 10.1371/journal.pcbi.1005185.

35. Morcos, A.S., and Harvey, C.D. (2016). History-dependent variability in population dynamics during evidence accumulation in cortex. Nat. Neurosci. *19*, 1672–1681. 10.1038/nn.4403.

36. Jazayeri, M., and Afraz, A. (2017). Navigating the Neural Space in Search of the Neural Code. Neuron *93*, 1003–1014. 10.1016/j.neuron.2017.02.019.

37. Pitkow, X., and Angelaki, D.E. (2017). Inference in the Brain: Statistics Flowing in Redundant Population Codes. Neuron *94*, 943–953. 10.1016/j.neuron.2017.05.028.

38. Stringer, C., Pachitariu, M., Steinmetz, N., Carandini, M., and Harris, K.D. (2019). High-dimensional geometry of population responses in visual cortex. Nature *571*, 361–365. 10.1038/s41586-019-1346-5.

39. Rajan, K., and Bialek, W. (2013). Maximally informative “stimulus energies” in the analysis of neural responses to natural signals. PloS One *8*, e71959. 10.1371/journal.pone.0071959.

40. Ecker, A.S., Berens, P., Cotton, R.J., Subramaniyan, M., Denfield, G.H., Cadwell, C.R., Smirnakis, S.M., Bethge, M., and Tolias, A.S. (2014). State dependence of noise correlations in macaque primary visual cortex. Neuron *82*, 235–248. 10.1016/j.neuron.2014.02.006.

41. Ruff, D.A., Xue, C., Kramer, L.E., Baqai, F., and Cohen, M.R. (2020). Low rank mechanisms underlying flexible visual representations. Proc. Natl. Acad. Sci. *117*, 29321–29329. 10.1073/pnas.2005797117.

42. Astorga, G., Chen, M., Yan, Y., Altavini, T.S., Jiang, C.S., Li, W., and Gilbert, C. (2022). Adaptive processing and perceptual learning in visual cortical areas V1 and V4. Proc. Natl. Acad. Sci. *119*, e2213080119. 10.1073/pnas.2213080119.

43. Roe, A.W., Chelazzi, L., Connor, C.E., Conway, B.R., Fujita, I., Gallant, J.L., Lu, H., and Vanduffel, W. (2012). Toward a Unified Theory of Visual Area V4. Neuron *74*, 12–29. 10.1016/j.neuron.2012.03.011.

44. Zeki, S., and Campbell, F.W. (1997). The distribution of wavelength and orientation selective cells in different areas of monkey visual cortex. Proc. R. Soc. Lond. B Biol. Sci. *217*, 449–470. 10.1098/rspb.1983.0020.

45. Bushnell, B.N., Harding, P.J., Kosai, Y., Bair, W., and Pasupathy, A. (2011). Equiluminance Cells in Visual Cortical Area V4. J. Neurosci. *31*, 12398–12412. 10.1523/JNEUROSCI.1890-11.2011.

46. Pasupathy, A., and Connor, C.E. (2001). Shape Representation in Area V4: Position-Specific Tuning for Boundary Conformation. J. Neurophysiol. *86*, 2505–2519. 10.1152/jn.2001.86.5.2505.

47. Hegdé, J., and Van Essen, D.C. (2005). Role of Primate Visual Area V4 in the Processing of 3-D Shape Characteristics Defined by Disparity. J. Neurophysiol. *94*, 2856–2866. 10.1152/jn.00802.2004.

48. Hinkle, D.A., and Connor, C.E. (2002). Three-dimensional orientation tuning in macaque area V4. Nat. Neurosci. *5*, 665–670. 10.1038/nn875.

49. Tolias, A.S., Keliris, G.A., Smirnakis, S.M., and Logothetis, N.K. (2005). Neurons in macaque area V4 acquire directional tuning after adaptation to motion stimuli. Nat. Neurosci. *8*, 591–593. 10.1038/nn1446.

50. Srinath, R., Emonds, A., Wang, Q., Lempel, A.A., Dunn-Weiss, E., Connor, C.E., and Nielsen, K.J. (2021). Early Emergence of Solid Shape Coding in Natural and Deep Network Vision. Curr. Biol. *31*, 51-65.e5. 10.1016/j.cub.2020.09.076.

51. Janssen, P., Verhoef, B.-E., and Premereur, E. (2018). Functional interactions between the macaque dorsal and ventral visual pathways during three-dimensional object vision. Cortex J. Devoted Study Nerv. Syst. Behav. *98*, 218–227. 10.1016/j.cortex.2017.01.021.

52. Pospisil, D.A., Pasupathy, A., and Bair, W. (2018). “Artiphysiology” reveals V4-like shape tuning in a deep network trained for image classification. eLife *7*, e38242. 10.7554/eLife.38242.

53. Bashivan, P., Kar, K., and DiCarlo, J.J. (2019). Neural population control via deep image synthesis. Science *364*. 10.1126/science.aav9436.

54. Oleskiw, T.D., Nowack, A., and Pasupathy, A. (2018). Joint coding of shape and blur in area V4. Nat. Commun. *9*, 466. 10.1038/s41467-017-02438-8.

55. El-Shamayleh, Y., and Pasupathy, A. (2016). Contour curvature as an invariant code for objects in visual area V4. J. Neurosci. *36*, 5532–5543. 10.1523/JNEUROSCI.4139-15.2016.

56. Kramer, L.E., Chen, Y.-C., Long, B., Konkle, T., and Cohen, M.R. (2023). Contributions of early and mid-level visual cortex to high-level object categorization. Preprint at bioRxiv, 10.1101/2023.05.31.541514 10.1101/2023.05.31.541514.

57. Long, B., Yu, C.-P., and Konkle, T. (2018). Mid-level visual features underlie the high-level categorical organization of the ventral stream. Proc. Natl. Acad. Sci. U. S. A. *115*, E9015–E9024. 10.1073/pnas.1719616115.

58. Wang, R., Janini, D., and Konkle, T. (2022). Mid-level feature differences underlie early animacy and object size distinctions: Evidence from EEG decoding. Preprint at bioRxiv, 10.1101/2022.01.12.475180 10.1101/2022.01.12.475180.

59. DiCarlo, J.J., and Cox, D.D. (2007). Untangling invariant object recognition. Trends Cogn. Sci. *11*, 333–341. 10.1016/j.tics.2007.06.010.

60. Hong, H., Yamins, D.L.K., Majaj, N.J., and DiCarlo, J.J. (2016). Explicit information for category-orthogonal object properties increases along the ventral stream. Nat. Neurosci. *19*, 613–622. 10.1038/nn.4247.

61. Cadieu, C.F., Hong, H., Yamins, D.L., Pinto, N., Ardila, D., Solomon, E.A., Majaj, N.J., and DiCarlo, J.J. (2014). Deep neural networks rival the representation of primate IT cortex for core visual object recognition. PLoS Comput. Biol. *10*, e1003963.

62. Majaj, N.J., Hong, H., Solomon, E.A., and DiCarlo, J.J. (2015). Simple Learned Weighted Sums of Inferior Temporal Neuronal Firing Rates Accurately Predict Human Core Object Recognition Performance. J. Neurosci. *35*, 13402–13418. 10.1523/JNEUROSCI.5181-14.2015.

63. Reynolds, D., and Singh, V. (2023). Characterization of human lightness discrimination thresholds for independent spectral variations. Preprint at bioRxiv, 10.1101/2023.06.16.545355 10.1101/2023.06.16.545355.

64. Singh, V., Burge, J., and Brainard, D.H. (2022). Equivalent noise characterization of human lightness constancy. J. Vis. *22*, 2. 10.1167/jov.22.5.2.

65. Rust, N.C., and Dicarlo, J.J. (2010). Selectivity and tolerance ("invariance") both increase as visual information propagates from cortical area V4 to IT. J. Neurosci. *30*, 12978–12995. 10.1523/JNEUROSCI.0179-10.2010.

66. DiCarlo, J.J., Zoccolan, D., and Rust, N.C. (2012). How does the brain solve visual object recognition? Neuron *73*, 415–434. 10.1016/j.neuron.2012.01.010.

67. Pagan, M., Urban, L.S., Wohl, M.P., and Rust, N.C. (2013). Signals in inferotemporal and perirhinal cortex suggest an untangling of visual target information. Nat. Neurosci. *16*, 1132–1139. 10.1038/nn.3433.

68. Yamins, D.L.K., Hong, H., Cadieu, C.F., Solomon, E.A., Seibert, D., and DiCarlo, J.J. (2014). Performance-optimized hierarchical models predict neural responses in higher visual cortex. Proc. Natl. Acad. Sci. U. S. A. *111*, 8619–8624. 10.1073/pnas.1403112111.

69. Hénaff, O.J., Goris, R.L.T., and Simoncelli, E.P. (2019). Perceptual straightening of natural videos. Nat. Neurosci. *22*, 984–991. 10.1038/s41593-019-0377-4.

70. Kriegeskorte, N., and Wei, X.-X. (2021). Neural tuning and representational geometry. Nat. Rev. Neurosci. *22*, 703–718. 10.1038/s41583-021-00502-3.

71. Fusi, S., Miller, E.K., and Rigotti, M. (2016). Why neurons mix: high dimensionality for higher cognition. Curr. Opin. Neurobiol. *37*, 66–74. 10.1016/j.conb.2016.01.010.

72. Rigotti, M., Barak, O., Warden, M.R., Wang, X.-J., Daw, N.D., Miller, E.K., and Fusi, S. (2013). The importance of mixed selectivity in complex cognitive tasks. Nature *497*, 585–590. 10.1038/nature12160.

73. Chung, S., Lee, D.D., and Sompolinsky, H. (2018). Classification and Geometry of General Perceptual Manifolds. Phys. Rev. X *8*, 031003. 10.1103/PhysRevX.8.031003.

74. Chung, S., and Abbott, L.F. (2021). Neural population geometry: An approach for understanding biological and artificial neural networks. Curr. Opin. Neurobiol. *70*, 137–144. 10.1016/j.conb.2021.10.010.

75. Cohen, U., Chung, S., Lee, D.D., and Sompolinsky, H. (2020). Separability and geometry of object manifolds in deep neural networks. Nat. Commun. *11*, 746. 10.1038/s41467-020-14578-5.

76. Jazayeri, M., and Ostojic, S. (2021). Interpreting neural computations by examining intrinsic and embedding dimensionality of neural activity. Curr. Opin. Neurobiol. *70*, 113–120. 10.1016/j.conb.2021.08.002.

77. Yuste, R. (2015). From the neuron doctrine to neural networks. Nat. Rev. Neurosci. *16*, 487–497. 10.1038/nrn3962.

78. Rajalingham, R., Issa, E.B., Bashivan, P., Kar, K., Schmidt, K., and DiCarlo, J.J. (2018). Large-Scale, High-Resolution Comparison of the Core Visual Object Recognition Behavior of Humans, Monkeys, and State-of-the-Art Deep Artificial Neural Networks. J. Neurosci. *38*, 7255–7269. 10.1523/JNEUROSCI.0388-18.2018.

79. Okazawa, G., Hatch, C.E., Mancoo, A., Machens, C.K., and Kiani, R. (2021). Representational geometry of perceptual decisions in the monkey parietal cortex. Cell *184*, 3748-3761.e18. 10.1016/j.cell.2021.05.022.

80. Ehrlich, D.B., and Murray, J.D. (2022). Geometry of neural computation unifies working memory and planning. Proc. Natl. Acad. Sci. *119*, e2115610119. 10.1073/pnas.2115610119.

81. Mante, V., Sussillo, D., Shenoy, K.V., and Newsome, W.T. (2013). Context-dependent computation by recurrent dynamics in prefrontal cortex. Nature *503*, 78–84. 10.1038/nature12742.

82. Bernardi, S., Benna, M.K., Rigotti, M., Munuera, J., Fusi, S., and Salzman, C.D. (2020). The Geometry of Abstraction in the Hippocampus and Prefrontal Cortex. Cell *183*, 954-967.e21. 10.1016/j.cell.2020.09.031.

83. Russo, A.A., Bittner, S.R., Perkins, S.M., Seely, J.S., London, B.M., Lara, A.H., Miri, A., Marshall, N.J., Kohn, A., Jessell, T.M., et al. (2018). Motor Cortex Embeds Muscle-like Commands in an Untangled Population Response. Neuron *97*, 953-966.e8. 10.1016/j.neuron.2018.01.004.

84. Gallego, J.A., Perich, M.G., Naufel, S.N., Ethier, C., Solla, S.A., and Miller, L.E. (2018). Cortical population activity within a preserved neural manifold underlies multiple motor behaviors. Nat. Commun. *9*, 4233. 10.1038/s41467-018-06560-z.

85. Sussillo, D., Churchland, M.M., Kaufman, M.T., and Shenoy, K.V. (2015). A neural network that finds a naturalistic solution for the production of muscle activity. Nat. Neurosci. *18*, 1025–1033. 10.1038/nn.4042.

86. Shenoy, K.V., Sahani, M., and Churchland, M.M. (2013). Cortical control of arm movements: a dynamical systems perspective. Annu. Rev. Neurosci. *36*, 337–359. 10.1146/annurev-neuro-062111-150509.

87. Khaligh-Razavi, S.-M., and Kriegeskorte, N. (2014). Deep supervised, but not unsupervised, models may explain IT cortical representation. PLoS Comput. Biol. *10*, e1003915. 10.1371/journal.pcbi.1003915.

88. Chung, S., Lee, D.D., and Sompolinsky, H. (2016). Linear readout of object manifolds. Phys. Rev. E *93*, 060301. 10.1103/PhysRevE.93.060301.

89. Zhou, H., Friedman, H.S., and Heydt, R. von der (2000). Coding of Border Ownership in Monkey Visual Cortex. J. Neurosci. *20*, 6594–6611. 10.1523/JNEUROSCI.20-17-06594.2000.

90. Maheswaranathan, N., McIntosh, L.T., Tanaka, H., Grant, S., Kastner, D.B., Melander, J.B., Nayebi, A., Brezovec, L.E., Wang, J.H., Ganguli, S., et al. (2023). Interpreting the retinal neural code for natural scenes: From computations to neurons. Neuron *111*, 2742-2755.e4. 10.1016/j.neuron.2023.06.007.

91. Ding, X., Lee, D., Melander, J.B., Sivulka, G., Ganguli, S., and Baccus, S.A. (2023). Information Geometry of the Retinal Representation Manifold. bioRxiv, 2023.05.17.541206. 10.1101/2023.05.17.541206.

92. Cowley, B.R., Stan, P.L., Pillow, J.W., and Smith, M.A. (2023). Compact deep neural network models of visual cortex. Preprint at bioRxiv, 10.1101/2023.11.22.568315 10.1101/2023.11.22.568315.

93. Felsen, G., and Dan, Y. (2005). A natural approach to studying vision. Nat. Neurosci. *8*, 1643–1646. 10.1038/nn1608.

94. Brainard, D.H. (1997). The Psychophysics Toolbox. Spat. Vis. *10*, 433–436.

95. Prins, N., and Kingdom, F.A.A. (2018). Applying the Model-Comparison Approach to Test Specific Research Hypotheses in Psychophysical Research Using the Palamedes Toolbox. Front. Psychol. *9*.

96. Lian, T., MacKenzie, K.J., Brainard, D.H., Cottaris, N.P., and Wandell, B.A. (2019). Ray tracing 3D spectral scenes through human optics models. J. Vis. *19*, 23. 10.1167/19.12.23.

97. Heasly, B.S., Cottaris, N.P., Lichtman, D.P., Xiao, B., and Brainard, D.H. (2014). RenderToolbox3: MATLAB tools that facilitate physically based stimulus rendering for vision research. J. Vis. *14*, 6. 10.1167/14.2.6.

98. Brainard, D., Jiang, H., Cottaris, N.P., Rieke, F., Chichilnisky, E.J., Farrell, J.E., and Wandell, B.A. (2015). ISETBIO: Computational tools for modeling early human vision. In Imaging and Applied Optics 2015 (2015), paper IT4A.4 (Optica Publishing Group), p. IT4A.4. 10.1364/ISA.2015.IT4A.4.

99. Foundation, B. blender.org - Home of the Blender project - Free and Open 3D Creation Software. blender.org. https://www.blender.org/.

100. Gardner, J.L., Merriam, E.P., Schluppeck, D., and Larsson, J. (2018). MGL: Visual psychophysics stimuli and experimental design package. Version 2.0 (Zenodo). 10.5281/zenodo.1299497 10.5281/zenodo.1299497.

101. Physically Based Rendering: From Theory to Implementation https://pbr-book.org/4ed/contents.

102. Pharr, M. (2024). mmp/pbrt-v3.